ChemPhysChem

Research Article
doi.org/10.1002/cphc.202300934

Chemistry Europe
European Chemical Societies Publishing

www.chemphyschem.org

Local Structure in Disordered Melilite Revealed by Ultrahigh Field ^{71}Ga and ^{139}La Solid-State Nuclear Magnetic Resonance Spectroscopy

Lucia Corti,[a, b] Ivan Hung,[c] Amrit Venkatesh,[c] Peter L. Gor'kov,[c] Zhehong Gan,[c] John B. Claridge,[a, b] Matthew J. Rosseinsky,[a, b] and Frédéric Blanc*[a, b, d]

Multinuclear Nuclear Magnetic Resonance (NMR) spectroscopy of quadrupolar nuclei at ultrahigh magnetic field provides compelling insight into the short-range structure in a family of fast oxide ion electrolytes with $La_{1+x}Sr_{1-x}Ga_3O_{7+0.5x}$ melilite structure. The striking resolution enhancement in the solid-state ^{71}Ga NMR spectra measured with the world's unique series connected hybrid magnet operating at 35.2 T distinctly resolves Ga sites in four- and five-fold coordination environments. Detection of five-coordinate Ga centers in the site-disordered $La_{1.54}Sr_{0.46}Ga_3O_{7.27}$ melilite is critical given that the GaO_5 unit accommodates interstitial oxide ions and provides excellent transport properties. This work highlights the importance of ultrahigh magnetic fields for the detection of otherwise broad spectral features in systems containing quadrupolar nuclei and the potential of ensemble-based computational approaches for the interpretation of NMR data acquired for site-disordered materials.

Introduction

Oxide ion conductors are a key component of Solid Oxide Fuel Cells (SOFCs), enabling the clean electrochemical conversion of a wide range of fuels. Nevertheless, the elevated temperatures required for efficient oxygen conduction in SOFCs hinders their large-scale employment.[1] For instance, the Y_2O_3 stabilized ZrO_2 electrolyte requires temperatures in the 800 °C to 1000 °C range to effectively conduct oxide ions, and this has prompted a search for novel electrolyte materials exhibiting enhanced ion conductivity at reduced temperatures.[1,2]

The melilite family of fast oxide ion conductors with $La_{1+x}Sr_{1-x}Ga_3O_{7+0.5x}$ composition has drawn considerable attention due to the excellent ionic transport properties of the La^{3+}-doped phase $La_{1.54}Sr_{0.46}Ga_3O_{7.27}$ in the 600 °C to 800 °C temperature range.[3,4] $LaSrGa_3O_7$ ($x=0$) consists of La^{3+}/Sr^{2+} cationic layers alternated with anionic layers composed of corner-sharing four-connected Ga(1)O_4 and three-connected Ga(2)O_4 tetrahedra (Figure 1a),[5] and the La^{3+}-doped $La_{1.54}Sr_{0.46}Ga_3O_{7.27}$ phase is distinguished by the additional presence of interstitial oxide ions accommodated in a distorted trigonal bipyramidal Ga(2′)O_5 structural unit (Figure 1b).[3]

The sensitivity of solid-state Nuclear Magnetic Resonance (NMR) spectroscopy to the short-range structure makes this technique ideal to detect local distortions induced by the presence of defects in disordered materials, thus providing complementary information to the average, long-range structure yielded by diffraction-based measurements. Magic Angle Spinning (MAS) NMR spectroscopy has proven to be an extremely powerful technique to gain insight into disorder and oxygen transport in $La_{1+x}Sr_{1-x}Ga_3O_{7+0.5x}$. However, the structural details encoded in the ^{71}Ga (spin quantum number $I=\frac{3}{2}$) MAS NMR spectra of these disordered phases are hindered by the presence of several broad and significantly overlapped resonances, even when performing the experiments at an external magnetic field strength B_0 up to 18.8 T and under fast MAS rates ν_r up to 60 kHz.[6] In fact, the NMR-active isotopes in $La_{1+x}Sr_{1-x}Ga_3O_{7+0.5x}$ are subject to strong quadrupolar interactions which result in anisotropically broadened NMR resonances, and this can have a severe impact on the resolution and utility of the data, especially for particularly challenging nuclei such as ^{139}La, ^{87}Sr and ^{71}Ga.[7,8]

In this work, we show that the 36 T Series Connected Hybrid (SCH) magnet[9] available at the National High Magnetic Field Laboratory (NHMFL) in Tallahassee (Florida, USA) equipped with the recently developed 1.3 mm solid-state NMR probe spinning at $\nu_r=60$ kHz yields impressive spectral resolution enhancement that is crucial to unambiguously observe and

[a] L. Corti, Prof. J. B. Claridge, Prof. M. J. Rosseinsky, Prof. F. Blanc
Department of Chemistry, University of Liverpool
Liverpool L69 7ZD, UK
E-mail: frederic.blanc@liverpool.ac.uk

[b] L. Corti, Prof. J. B. Claridge, Prof. M. J. Rosseinsky, Prof. F. Blanc
Leverhulme Research Centre for Functional Materials Design, Materials Innovation Factory, University of Liverpool
Liverpool L69 7ZD, UK

[c] Dr. I. Hung, Dr. A. Venkatesh, Dr. P. L. Gor'kov, Dr. Z. Gan
National High Magnetic Field Laboratory,
Florida State University,
Tallahassee FL 32310, USA

[d] Prof. F. Blanc
Stephenson Institute for Renewable Energy,
University of Liverpool
Liverpool L69 7ZF, UK

Supporting information for this article is available on the WWW under https://doi.org/10.1002/cphc.202300934

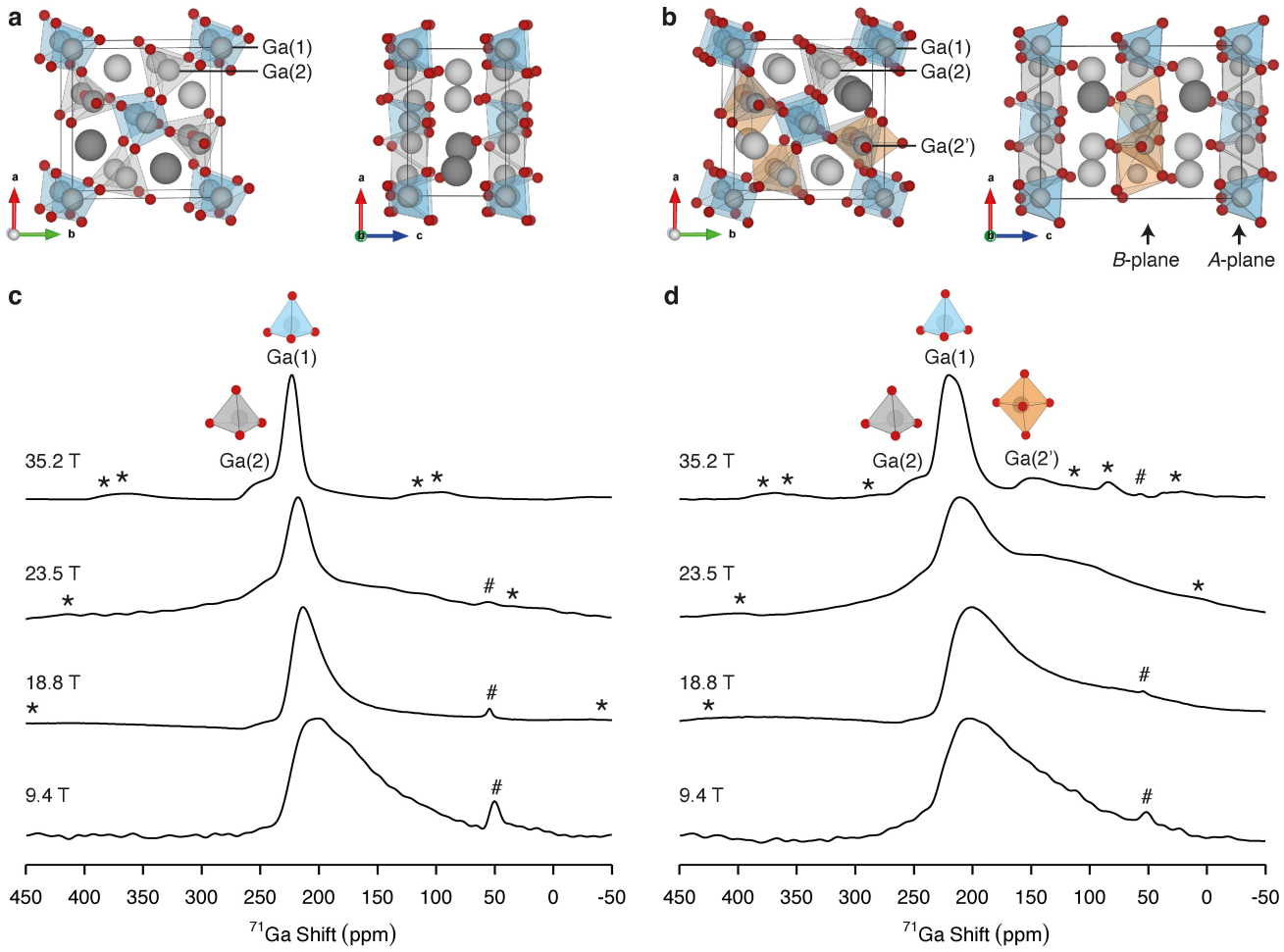

Figure 1. Example of symmetrically inequivalent configurations viewed along the *c*-axis (left) and *b*-axis (right) and generated for (a) a disordered $LaSrGa_3O_7$ 1×1×1 unit cell and (b) a disordered $La_{1.5}Sr_{0.5}Ga_3O_{7.25}$ 1×1×2 supercell, showing four-connected Ga(1)O_4 (blue), three-connected Ga(2)O_4 (gray) and Ga(2′)O_5 (orange) polyhedra. *A*-planes (without interstitial defects) and *B*-planes (containing interstitial defects accommodated in Ga(2′)O_5 structural units) perpendicular to the *c*-axis are highlighted. O, Sr and La atoms are respectively shown in red, dark gray and light gray. One-dimensional ^{71}Ga MAS NMR spectra of (c) $LaSrGa_3O_7$ and (d) $La_{1.54}Sr_{0.46}Ga_3O_{7.27}$ recorded at 9.4 T,[6] 18.8 T,[6] 23.5 T and 35.2 T under $\nu_r = 60$ kHz. Isolated GaO_n polyhedra are shown above the corresponding ^{71}Ga signals. Data at 35.2 T were recorded with the rotor-synchronized QCPMG sequence processed with co-added echoes. QCPMG data processed with direct Fourier transformation are shown in Figure S2. The asterisks (*) denote the spinning sidebands, and the hash symbols (#) indicate the signal assigned to a La(Sr)GaO_3 impurity.[6]

assign the ^{71}Ga NMR resonances of $LaSrGa_3O_7$ and $La_{1.54}Sr_{0.46}Ga_3O_{7.27}$. Furthermore, static ^{139}La ($I = \frac{7}{2}$) NMR data are reported for the first time at 35.2 T and provide further insight into the local structure of these phases. Comparison of data recorded for the parent $LaSrGa_3O_7$ phase (only containing framework oxide ions) and the La^{3+}-doped $La_{1.54}Sr_{0.46}Ga_3O_{7.27}$ phase (also containing interstitial oxide ions) enables the identification of structural differences arising from the introduction of defects into the lattice.

Results and Discussion

Figure 1c–d presents a comparison of the ^{71}Ga MAS NMR spectra of $LaSrGa_3O_7$ and $La_{1.54}Sr_{0.46}Ga_3O_{7.27}$ recorded at 9.4 T,[6] 18.8 T,[6] 23.5 T, and 35.2 T. The fast MAS rates enabled by the new 1.3 mm probe prevent overlap between signals and spinning sidebands, offering an alternative to more specialized approaches such as the Quadrupolar Magic-Angle Turning (QMAT) experiment.[10] The second-order quadrupolar broadening combined with a distribution of chemical shifts typical of disordered systems results in broad ^{71}Ga NMR resonances, especially at 9.4 T, as also observed in previous ^{71}Ga MAS NMR experiments on $LaSrGa_3O_7$ at 23.5 T under ν_r of 30 kHz[11] and related melilite phases.[12–14] Striking resolution enhancement is observed as B_0 is increased up to 35.2 T owing to the inverse proportionality of the second-order quadrupolar broadening to B_0 in Hz and B_0^2 in ppm, thus enabling the identification of several resonances which are unresolved at lower B_0. In particular, the remarkable spectral resolution achieved at 35.2 T allows the unambiguous detection of two ^{71}Ga resonances in the ^{71}Ga Quadrupolar Carr-Purcell-Meiboom-Gill (QCPMG)[15,16] spectrum of $LaSrGa_3O_7$. One signal appears at a shift δ of ~223 ppm and is relatively sharp, while the other resonance is observed at ~230 ppm and is significantly broader (Figure 1c). More importantly, one additional signal at a much lower δ of

~145 ppm is further revealed in the ^{71}Ga NMR spectrum of the La^{3+}-doped $La_{1.54}Sr_{0.46}Ga_3O_{7.27}$ phase (Figure 1d).

Interpretation of NMR spectra featuring intricate spectral line shapes is often guided by the computation of NMR parameters.[17–19] However, the computational modeling of the melilite phases is challenged by their configurational complexity arising from site disorder. An ensemble-based approach[20,21] is therefore utilized to capture the mixed site occupancies of the La^{3+}/Sr^{2+} sites and the partial site occupancy of the interstitial site O(4). Figure 2a–b shows the ^{71}Ga MAS NMR spectra simulated at 35.2 T from the NMR parameters previously[6] computed with the Gauge Including Projector Augmented Waves (GIPAW)-Density Functional Theory (DFT) approach[17,18,22] for an ensemble of symmetrically inequivalent configurations with $LaSrGa_3O_7$ and $La_{1.5}Sr_{0.5}Ga_3O_{7.25}$ stoichiometries (further computational details are provided in the Experimental Section).[20] Firstly, the excellent agreement observed between the experimental and computed ^{71}Ga NMR spectra validates the potential of ensemble-based approaches to model mixed and partial site occupancies in disordered materials, especially when utilized in conjunction with experimental NMR spectroscopy. Secondly, inspection of the contributions of the distinct Ga environments to the overall computed spectrum reveals clear assignment of the spectral features. In particular, the relatively sharp signal at δ of ~223 ppm and the broader resonance at ~230 ppm are assigned to the four-connected $Ga(1)O_4$ and three-connected $Ga(2)O_4$ tetrahedra, respectively, while the ^{71}Ga NMR signal at ~145 ppm exclusively observed for $La_{1.54}Sr_{0.46}Ga_3O_{7.27}$ is attributed to the five-coordinate trigonal bipyramidal $Ga(2')O_5$ structural unit. This confirms that the interstitial oxide ions in $La_{1.54}Sr_{0.46}Ga_3O_{7.27}$ are located in the pentagonal channels formed by the edges of two $Ga(1)O_4$ and three $Ga(2)O_4$ tetrahedra and accommodated in a GaO_5 structural unit (Figure 1b).

Closer inspection of the ^{71}Ga MAS NMR spectra (Figure 2) computed at 35.2 T reveals the presence of two partially overlapping Ga(1) resonances for both $LaSrGa_3O_7$ and $La_{1.5}Sr_{0.5}Ga_3O_{7.25}$ which were previously unresolved in the spectra simulated at 18.8 T.[6] Notably, the two Ga(1) resonances are not resolved in the corresponding experimental spectra at 35.2 T, motivating further investigation of the origin of these spectral features. While the two Ga(1) resonances computed for $LaSrGa_3O_7$ are characterized by similar quadrupolar coupling constants (C_Q) and originate from different distributions of the La^{3+}/Sr^{2+} cations in the two symmetrically inequivalent configurations (Figures 3a and S1), the two Ga(1) signals resolved in the $La_{1.5}Sr_{0.5}Ga_3O_{7.25}$ spectrum arise from Ga(1) sites in either the *A*-plane (not containing the interstitial defect) or *B*-plane (containing the interstitial defect) illustrated in Figure 1b. The C_Q and isotropic chemical shift $\delta_{iso,cs}$ values computed for Ga(1) sites in the *A*-plane are respectively smaller and larger than those calculated for Ga(1) sites in the *B*-plane, as highlighted in Figure 3a. The two Ga(1) resonances are not distinctly resolved in the $La_{1.54}Sr_{0.46}Ga_3O_{7.27}$ experimental spectrum, although a shoulder at lower frequencies is visible (Figure 2b). This discrepancy between the experimental and computational $La_{1.54}Sr_{0.46}Ga_3O_{7.27}$ data likely arises because the number of structural models composing the configurational ensemble is limited by the size of the supercell (1×1×2) (Figure 1b). Using a larger supercell expansion with more than one interstitial oxide ion would give rise to an additional degree of freedom given by the proximity of the interstitials, but it would also prohibitively increase the computational cost.

Two-dimensional ^{71}Ga Triple-Quantum Magic Angle Spinning (3QMAS) experiments of $LaSrGa_3O_7$ and $La_{1.54}Sr_{0.46}Ga_3O_{7.27}$ were performed at 35.2 T in an attempt to obtain isotropic spectra. The experiments were recorded with the low-power Multiple Quantum Magic Angle Spinning (lpMQMAS) pulse sequence[24] which is specifically suited for large quadrupolar interactions (Figure 3b–c). In the lpMQMAS pulse sequence, 'composite' pulses consisting of on-resonance Central-Transition (CT)-selective pulses concatenated with off-resonance Satellite-Transition (ST)-selective inversion pulses substitute for the short, high-power pulses used in conventional MQMAS sequences to excite and convert triple-quantum coherences.[24] Only the Ga(1) signal appears in the ^{71}Ga 3QMAS spectra of both $LaSrGa_3O_7$

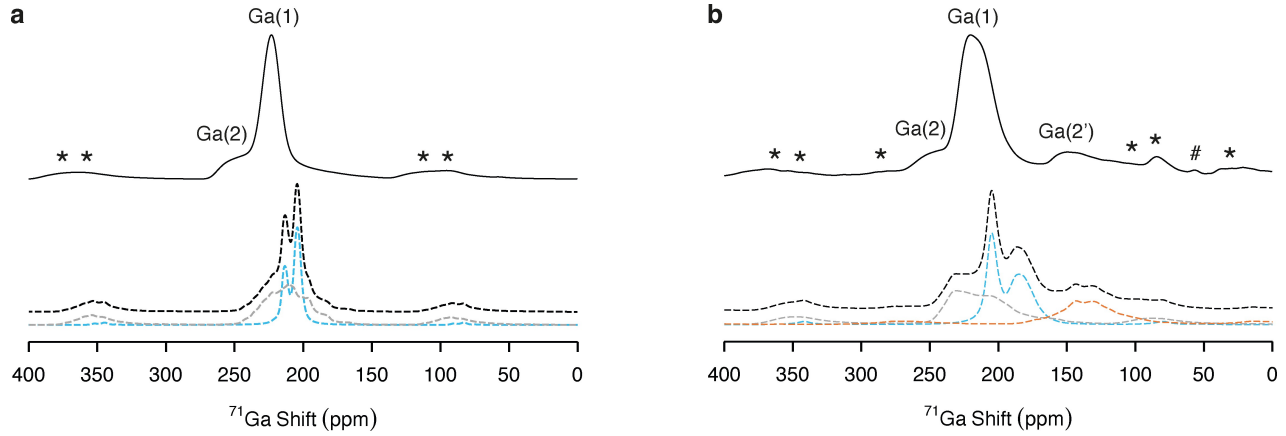

Figure 2. ^{71}Ga MAS NMR spectra of (a) $LaSrGa_3O_7$ and (b) $La_{1.54}Sr_{0.46}Ga_3O_{7.27}$ at 35.2 T. The experimental spectra (solid black line) are shown above the computed spectra (dashed black line).[23] The colored lines indicate the contribution of Ga(1) (blue), Ga(2) (gray) and Ga(2') (orange) sites to the overall computed spectra. The asterisks (*) denote the spinning sidebands, and the hash symbol (#) indicates the signal assigned to a $La(Sr)GaO_3$ impurity.[6] Details regarding the computed spectra are provided in the Experimental Section.

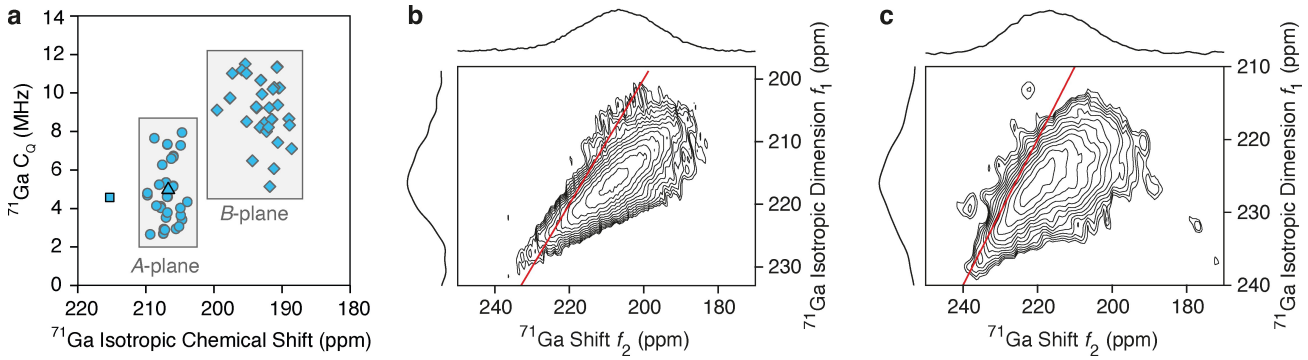

Figure 3. (a) ^{71}Ga quadrupolar coupling constants (C_Q) vs. ^{71}Ga isotropic chemical shifts computed[6] using an ensemble-based approach[20] for the $LaSrGa_3O_7$ Ga(1) sites in the two distinct symmetrically inequivalent configurations (square and triangle with black borders) and for the $La_{1.5}Sr_{0.5}Ga_3O_{7.25}$ Ga(1) sites in the *A*- and *B*-planes (circles and diamonds with gray borders, respectively). ^{71}Ga lpMQMAS spectra of (b) $LaSrGa_3O_7$ and (c) $La_{1.54}Sr_{0.46}Ga_3O_{7.27}$ at 35.2T after shearing the f_1 dimension into an isotropic representation. Exemplary slices parallel to the f_2 dimension are shown in Figure S3. The red diagonal line with slope 1 provides visual guidance for assessing the strength of the quadrupolar interactions.

and $La_{1.54}Sr_{0.46}Ga_3O_{7.27}$ despite (i) the ability of the lpMQMAS pulse sequence to efficiently interconvert CT and triple-quantum coherences for large quadrupolar couplings[24] and (ii) the sufficiently long transverse relaxation time constants T_2' (estimated from the decay of the QCPMG echo train to be approximately 60 ms for $LaSrGa_3O_7$ and 5 ms for $La_{1.54}Sr_{0.46}Ga_3O_{7.27}$). This is surprising at first glance given that, for instance, the ^{71}Ga signals of the completely ordered, fully substituted $La_2Ga_3O_{7.5}$ melilite phase could be resolved in the related ^{71}Ga Satellite-Transition Magic Angle Spinning (STMAS) spectrum at 20 T under ν_r of 100 kHz.[25] The absence of the Ga(2)/Ga(2′) signals in the 3QMAS spectra of $LaSrGa_3O_7$ and $La_{1.54}Sr_{0.46}Ga_3O_{7.27}$ (Figure 3b–c) can be explained considering the significant difference in magnitude of the C_Q constants calculated for the Ga(1) and Ga(2)/Ga(2′) sites combined with the considerable distribution of the C_Q and $\delta_{iso,cs}$ values obtained for Ga(2)/Ga(2′) which arises from the presence of disorder, as shown in previous work (e.g., $\sim$2.7 MHz $< |C_Q|_{Ga(1)} <$ $\sim$11.4 MHz and $\sim$3.2 MHz $< |C_Q|_{Ga(2)/Ga(2')} <$ $\sim$23.7 MHz for $La_{1.54}Sr_{0.46}Ga_3O_{7.27}$).[6] This results in large differences in intensity between the Ga(1) and Ga(2)/Ga(2′) signals in both the direct and indirect dimensions of the 3QMAS spectra, thereby challenging the detection of the low-intensity signals. Nevertheless, the shape of the signals in the 3QMAS spectra reveals that Ga(1) sites featuring larger C_Q constants present smaller $\delta_{iso,cs}$ values, as observed by a larger deviation of spectra intensity from the diagonal at lower chemical shifts. This is in agreement with the trend in NMR parameters computed for the Ga(1) sites in the *A*- and *B*-planes discussed above.

To investigate configurational disorder, static ^{139}La QCPMG spectra were also recorded at 35.2 T (Figure 4a–b). Relatively broad signals with breadths of approximately 700 kHz are observed for both $LaSrGa_3O_7$ and $La_{1.54}Sr_{0.46}Ga_3O_{7.27}$ owing to the large nuclear electric quadrupole moment of ^{139}La (Q (^{139}La) = 0.206(4)×10^{28} m^2 as opposed to Q (^{71}Ga) = 0.107(1)×10^{28} m^2).[26–29] Comparison between the spectral lineshapes captured for $LaSrGa_3O_7$ and $La_{1.54}Sr_{0.46}Ga_3O_{7.27}$ is compelling evidence for enhanced disorder in the La^{3+}-doped phase. Despite the challenges associated with the computational treatment of heavy elements such as ^{139}La, the experimental data are importantly in close agreement with the ^{139}La spectra predicted from the NMR parameters computed using the ensemble-based approach presented above and the Zeroth-Order Regular Approximation (ZORA)[30] to treat scalar relativistic effects (Figure 4c–d). ^{139}La spectra were simulated for each symmetrically inequivalent configuration to investigate possible La^{3+}/Sr^{2+} cation ordering patterns in the melilite phases (Figures S4 and S5). Nevertheless, the absence of distinct features in the ^{139}La NMR spectrum of $La_{1.54}Sr_{0.46}Ga_3O_{7.27}$ challenges the identification of favorable cation ordering patterns.

Conclusions

In conclusion, high-resolution ^{71}Ga MAS NMR spectra of $La_{1+x}Sr_{1-x}Ga_3O_{7+0.5x}$ recorded at the highest possible magnetic field of 35.2 T enable the detection of resonances assigned to four-connected Ga(1)O_4, three-connected Ga(2)O_4 and Ga(2′)O_5 which were unresolved at lower magnetic field strengths. The detection of the Ga(2′)O_5 structural unit, only observed for $La_{1.54}Sr_{0.46}Ga_3O_{7.27}$, is of strong relevance because of the role the five-coordinate Ga center plays in the ionic transport mechanism, and this sheds light on the importance of ultrahigh magnetic fields to unravel structural details encoded in the NMR spectra of quadrupolar nuclei. While limited structural information can be deduced from the ^{139}La NMR data, the considerably different spectral lineshapes observed for $LaSrGa_3O_7$ and $La_{1.54}Sr_{0.46}Ga_3O_{7.27}$ are well reproduced by the ensemble-based computational approach, highlighting the potential of this methodology to model La-containing systems.

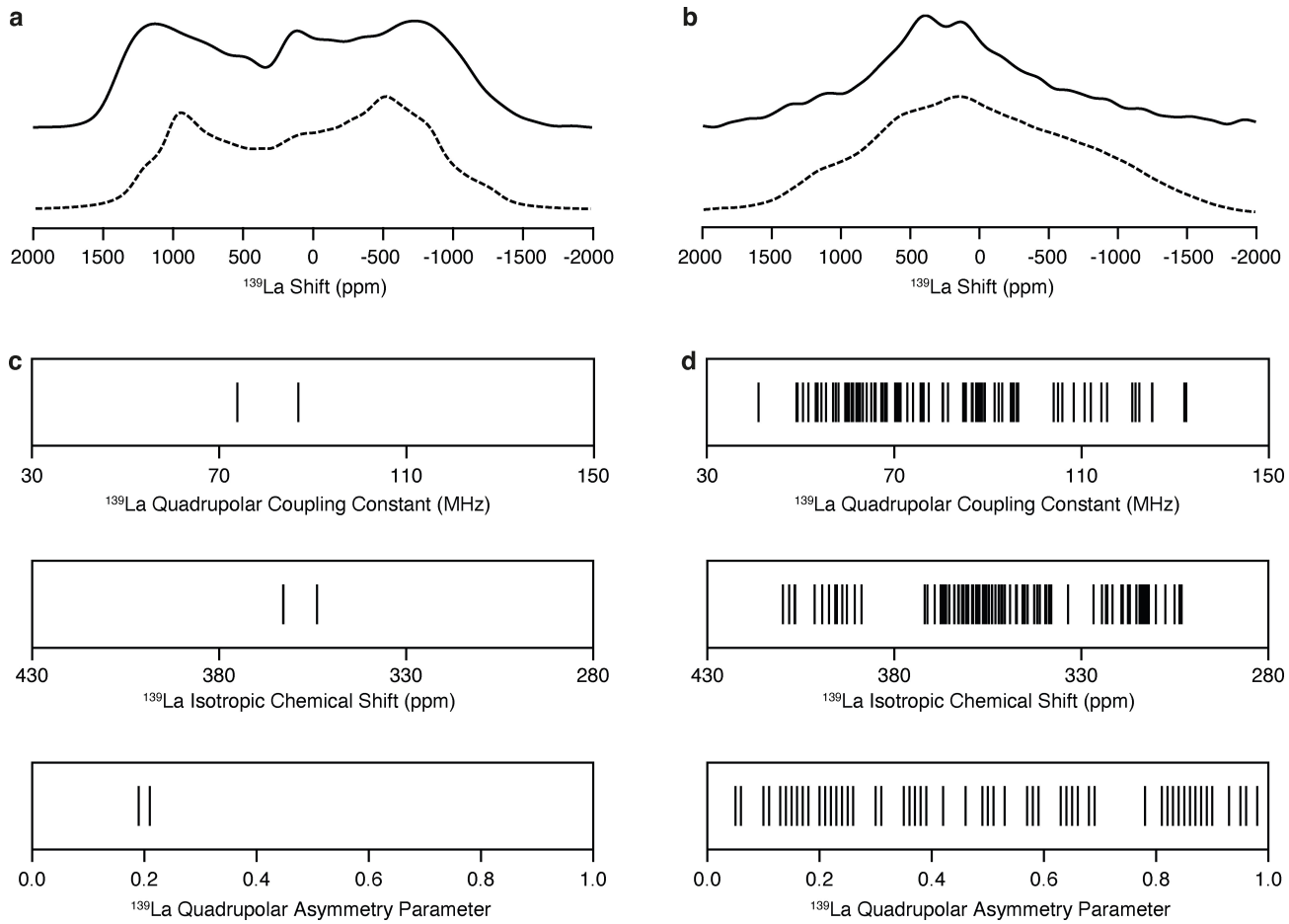

Figure 4. Experimental (solid line) and computed (dashed line) one-dimensional ^{139}La NMR spectra at 35.2 T of (a) $LaSrGa_3O_7$ and (b) $La_{1.54}Sr_{0.46}Ga_3O_{7.27}$ under static conditions. ^{139}La quadrupolar coupling constants, isotropic chemical shifts and quadrupolar asymmetry parameters of (c) $LaSrGa_3O_7$ and (d) $La_{1.54}Sr_{0.46}Ga_3O_{7.27}$ calculated for an ensemble of inequivalent configurations and used to generate the computed spectra. The computed spectra are obtained by summing the spectra simulated for each inequivalent configuration weighted by the configurational degeneracy. Details regarding the computed spectra are provided in the Experimental Section. Experimental data were recorded with the QCPMG sequence processed with co-added echoes. QCPMG data processed with direct Fourier transformation are shown in Figure S6.

Experimental Section

Materials Synthesis

The synthesis of the $LaSrGa_3O_7$ and La^{3+}-doped $La_{1.54}Sr_{0.46}Ga_3O_{7.27}$ melilite samples was performed following a known procedure.[3] Samples contain a small amount of $La(Sr)GaO_3$ perovskite as revealed by powder X-ray diffraction patterns[6] and the ~56 ppm signal in the ^{71}Ga MAS NMR spectra.[31]

^{71}Ga Solid-State NMR Experiments

All ^{71}Ga MAS NMR experiments were performed at a MAS rate ν_r of 60 kHz using 1.3 mm rotors. One-dimensional ^{71}Ga MAS NMR spectra at 9.4 T and 18.8 T were acquired with single pulse and Hahn echo sequences, respectively, and using the experimental settings detailed in previous work.[6] One-dimensional ^{71}Ga MAS NMR spectra at 23.5 T were recorded on a Bruker Avance Neo NMR spectrometer equipped with a 1.3 mm double resonance HX probe tuned to X = ^{71}Ga at a Larmor frequency $\nu_0 = 305.09$ MHz, using the Hahn echo sequence and pulses with rf field amplitude ν_1 equal to 168 kHz. Ultrahigh field ^{71}Ga MAS NMR experiments were performed at the NHMFL in Tallahassee (Florida, USA) on a 36 T SCH spectrometer[9] operating at 35.2 T equipped with a 1.3 mm HXY probe built in-house and used in double-resonance mode. The stator assembly of the probe was designed at the NHMFL to accommodate standard Bruker 1.3 mm rotors. The probe was tuned to X = ^{71}Ga at $\nu_0 = 457.48$ MHz. One-dimensional ^{71}Ga MAS NMR experiments at 35.2 T were recorded using the rotor-synchronized QCPMG sequence[15,16] combined with an initial Wideband Uniform Rate Smooth Truncation (WURST) pulse[32] for signal enhancement. The duration of the $\pi/2$ excitation and π refocusing pulses was set to 2 μs and 4 μs, respectively. The 1 ms WURST pulse with sweep width of 60 kHz (i.e., equal to the MAS rate) was placed at an experimentally optimized frequency offset of either 500 kHz for $LaSrGa_3O_7$ or 600 kHz for $La_{1.54}Sr_{0.46}Ga_3O_{7.27}$, and the power of the frequency sweep was set to either 20 W (~23 kHz) for $LaSrGa_3O_7$ or 30 W (~28 kHz) for $La_{1.54}Sr_{0.46}Ga_3O_{7.27}$. The echoes were coadded and subsequently Fourier transformed to obtain the envelope of the spikelets. Quantitative one-dimensional ^{71}Ga data at 23.5 T and 35.2 T were acquired with recycle delays of 3 s for $LaSrGa_3O_7$ and 0.3 s for $La_{1.54}Sr_{0.46}Ga_3O_{7.27}$. Two dimensional 3QMAS experiments at 35.2 T were performed using the shifted-echo lp3QMAS sequence,[24] combined with an initial WURST pulse for signal enhancement. The duration of the on-resonance CT-selective $\pi/2$ and π pulses was set to 2 μs and 4 μs, respectively. Rotor period long (i.e., 16.667 μs) pulses τ_r were applied at a large offset of

$12\times\nu_r = 720$ kHz from the CT, thereby making them selective to the ST. The experimental parameters of the initial WURST pulse were kept the same as in the corresponding one-dimensional spectra. 10 rotor-synchronized t_1 increments were recorded, and the recycle delay was set to 0.5 s and 75 ms for $LaSrGa_3O_7$ and $La_{1.54}Sr_{0.46}Ga_3O_{7.27}$, respectively. ^{71}Ga NMR spectra at 9.4 T, 18.8 T and 23.5 T are reported relative to the ^{71}Ga signal of a 1 M solution of $Ga(NO_3)_3$ in H_2O at 0 ppm. ^{71}Ga NMR data at 35.2 T were externally calibrated to the ^{1}H chemical shift of alanine at 1.46 ppm (indirectly referenced to tetramethylsilane at 0 ppm) using the IUPAC frequency ratios.[33]

^{139}La Solid-State NMR Experiments

^{139}La solid-state NMR experiments were performed at the NHMFL on the SCH spectrometer[9] operating at 35.2 T and equipped with the 1.3 mm HXY probe in double-resonance mode tuned to X = ^{139}La at $\nu_0 = 211.90$ MHz. Static conditions were used owing to the breadths of the ^{139}La signals which substantially exceed the available MAS rates. One-dimensional data were acquired with the QCPMG sequence[15,16] setting the length of the excitation and refocusing pulses to 1.5 μs. Recycle delays of 1 s and 50 ms were used for $LaSrGa_3O_7$ and $La_{1.54}Sr_{0.46}Ga_3O_{7.27}$, respectively. ^{139}La NMR data at 35.2 T were externally calibrated to the ^{1}H chemical shift of alanine at 1.46 ppm (indirectly referenced to tetramethylsilane at 0 ppm) using the IUPAC frequency ratios.[33]

Computations

The ^{71}Ga and ^{139}La NMR parameters were computed with the GIPAW-DFT approach[17,18,22] for an ensemble of symmetrically inequivalent configurations generated with the Site Occupancy Disorder (SOD) program[20] from a $LaSrGa_3O_7$ 1×1×1 unit cell and a $La_{1.5}Sr_{0.5}Ga_3O_{7.25}$ 1×1×2 supercell (containing one interstitial oxide ion). Plane-wave DFT[22] with periodic boundary conditions was used to optimise the geometry of the 2 and 18 symmetrically inequivalent configurations respectively generated for $LaSrGa_3O_7$ and $La_{1.5}Sr_{0.5}Ga_3O_{7.25}$, allowing both the atomic coordinates and the unit cell parameters to vary. The NMR parameters were calculated employing the geometry-optimized structures. Ultrasoft pseudopotentials[34] generated on-the-fly and the Perdew-Burke-Ernzerhof (PBE) exchange-correlation functional[35] were used throughout. Scalar relativistic effects were treated with the ZORA approach.[30] An energy cutoff of 800 eV and a k-point grid[36] of 2×2×3 (for $LaSrGa_3O_7$) and 2×2×2 (for $La_{1.5}Sr_{0.5}Ga_3O_{7.25}$) were used. CASTEP (version 20.11)[37] was employed to carry out all calculations. The C_Q parameters for ^{139}La were calculated using the revised nuclear electric quadrupole moment Q (^{139}La) = $0.206(4)\times10^{28}$ m^2.[27–29] To facilitate comparison between computed and experimental results, the isotropic and anisotropic chemical shifts ($\delta_{iso,cs}$ and $\delta_{aniso,cs}$, respectively) were determined from the computed isotropic chemical shielding $\sigma_{iso,cs}$ and anisotropic chemical shielding $\sigma_{aniso,cs}$ using $\delta_{iso,cs} = \sigma_{ref} + m\sigma_{iso,cs}$ and $\delta_{aniso,cs} = m\sigma_{aniso,cs}$, with σ_{ref} (^{71}Ga) = 1442.22 ppm, m (^{71}Ga) = −0.821, σ_{ref} (^{139}La) = 3460.92 ppm and m (^{139}La) = −0.681. The σ_{ref} and m values were calculated using a standard procedure which also aims at reducing the systematic errors in the calculations.[38] SIMPSON[23] was employed to simulate the NMR spectra from the computed NMR parameters taking into consideration both the electric field gradient and chemical shift anisotropy tensors. Either the gcompute method (for MAS spectra) or the direct method (for spectra under static conditions) were used. The NMR spectra obtained for each configuration were weighted by the configurational degeneracy and summed to obtain the total spectrum in the high-temperature limit $e^{\Delta E/(k_B T)} \rightarrow 1$, as described in more details elsewhere.[6,21] Further computational details are reported in previous work.[6]

Acknowledgements

The authors thank Dr. Chris I. Thomas (University of Liverpool) for the synthesis of the $LaSrGa_3O_7$ and $La_{1.54}Sr_{0.46}Ga_3O_{7.27}$ samples. All calculations were performed on the Barkla high-performance computing cluster at the University of Liverpool. L. C. thanks the Leverhulme Trust for support from the Leverhulme Research Centre for Functional Materials Design for a Ph.D. studentship, also partially supported by the University of Liverpool. A portion of this work was performed at the National High Magnetic Field Laboratory, which is supported by National Science Foundation Cooperative Agreement No. DMR-2128556 and the State of Florida. Research reported in this publication was supported by the National Institute Of General Medical Sciences of the National Institutes of Health under Award Number P41GM122698 and RM1GM148766. The content is solely the responsibility of the authors and does not necessarily represent the official views of the National Institutes of Health. The UK High-Field Solid-State NMR Facility used in this research was funderd by EPSRC and BBSRC (EP/T015063/1), as well as, for the 1 GHz instrument, EP/R029946/1. Collaborative assistance from the Facility Manager Team (W. Trent Franks and Dinu Iuga, University of Warwick) is acknowledged. F. B. thanks the EPSRC for upgrading the 800 MHz spectrometer at the University of Liverpool (EP/S013393/1). M. J. R. thanks the Royal Society for a Research Professorship.

Conflict of Interests

The authors declare no conflict of interest.

Data Availability Statement

Research data supporting this work are accessible from the University of Liverpool Research Data Catalogue: https://doi.org/10.17638/datacat.liverpool.ac.uk/2540.

Keywords: density functional calculations · disorder · melilite · NMR spectroscopy · solid electrolytes

[1] E. D. Wachsman, K. T. Lee, *Science* **2011**, *334*, 935.
[2] H. Shi, C. Su, R. Ran, J. Cao, Z. Shao, *Prog. Nat. Sci.* **2020**, *30*, 764.
[3] X. Kuang, M. A. Green, H. Niu, P. Zajdel, C. Dickinson, J. B. Claridge, L. Jantsky, M. J. Rosseinsky, *Nat. Mater.* **2008**, *7*, 498.
[4] X. Yang, A. J. Fernández-Carrión, X. Kuang, *Chem. Rev.* **2023**, *123*, 9356.
[5] J. M. S. Skakle, R. Herd, *Powder Diffr.* **1999**, *14*, 195.
[6] L. Corti, D. Iuga, J. B. Claridge, M. J. Rosseinsky, F. Blanc, *J. Am. Chem. Soc.* **2023**, *145*, 21817.
[7] S. E. Ashbrook, *Phys. Chem. Chem. Phys.* **2009**, *11*, 6892.
[8] D. L. Bryce, *Dalton Trans.* **2019**, *48*, 8014.
[9] Z. Gan, I. Hung, X. Wang, J. Paulino, G. Wu, I. M. Litvak, P. L. Gorkov, W. W. Brey, P. Lendi, J. L. Schiano, M. D. Bird, I. R. Dixon, J. Toth, G. S. Boebinger, T. A. Cross, *J. Magn. Reson.* **2017**, *284*, 125.

[10] I. Hung, Z. Gan, *Chem. Phys. Lett.* **2010**, *496*, 162.
[11] C. Ferrara, C. Tealdi, P. Mustarelli, M. Hoelzel, A. J. Pell, G. Pintacuda, *J. Phys. Chem. C* **2014**, *118*, 15036.
[12] J. Xu, X. Li, F. Lu, H. Fu, C. M. Brown, X. Kuang, *J. Solid State Chem.* **2015**, *230*, 309.
[13] X. Li, X. Wei, X. Wang, C. Lou, W. Zhang, J. Xu, Z. Luo, M. Tang, S. Deng, L. He, X. Xing, J. Sun, X. Kuang, *J. Mater. Chem. A* **2023**, *11*, 5615.
[14] X. Wei, X. Li, X. Wang, J. Liu, Z. Luo, S. Deng, L. He, J. Sun, X. Kuang, X. Xing, *ACS Appl. Energ. Mater.* **2023**, *6*, 3986.
[15] H. Y. Carr, E. M. Purcell, *Phys. Rev.* **1954**, *94*, 630.
[16] S. Meiboom, D. Gill, *Rev. Sci. Instrum.* **1958**, *29*, 688.
[17] C. J. Pickard, F. Mauri, *Phys. Rev. B* **2001**, *63*, 245101.
[18] J. R. Yates, C. J. Pickard, F. Mauri, *Phys. Rev. B* **2007**, *76*, 024401.
[19] C. Bonhomme, C. Gervais, F. Babonneau, C. Coelho, F. Pourpoint, T. Azaïs, S. E. Ashbrook, J. M. Griffin, J. R. Yates, F. Mauri, C. J. Pickard, *Chem. Rev.* **2012**, *112*, 5733.
[20] R. Grau-Crespo, S. Hamad Gomez, R. Catlow, N. Leeuw, *J. Phys. Condens. Matter* **2007**, *19*, 256201.
[21] R. F. Moran, D. McKay, P. C. Tornstrom, A. Aziz, A. Fernandes, R. Grau-Crespo, S. E. Ashbrook, *J. Am. Chem. Soc.* **2019**, *141*, 17838.
[22] W. Kohn, L. J. Sham, *Phys. Rev.* **1965**, *140*, A1133.
[23] M. Bak, J. T. Rasmussen, N. C. Nielsen, *J. Magn. Reson.* **2000**, *147*, 296.
[24] I. Hung, Z. Gan, *J. Magn. Reson.* **2021**, *324*, 106913.
[25] J. Fan, V. Sarou-Kanian, X. Yang, M. Diaz-Lopez, F. Fayon, X. Kuang, M. Pitcher, M. Allix, *Chem. Mater.* **2020**, *32*, 9016.
[26] C. R. Jacob, L. Visscher, C. Thierfelder, P. Schwerdtfeger, *J. Chem. Phys.* **2007**, *127*, 204303.
[27] I. Itkin, E. Eliav, U. Kaldor, *Theor. Chem. Acc.* **2011**, *129*, 409.
[28] P. Pyykkö, *Mol. Phys.* **2018**, *116*, 1328.
[29] C. Leroy, P. M. Szell, D. L. Bryce, *Magn. Reson. Chem.* **2018**, *57*, 265.
[30] J. R. Yates, C. J. Pickard, M. C. Payne, F. Mauri, *J. Chem. Phys.* **2003**, *118*, 5746.
[31] F. Blanc, D. S. Middlemiss, Z. Gan, C. P. Grey, *J. Am. Chem. Soc.* **2011**, *133*, 17662.
[32] E. Kupce, R. Freeman, *J. Magn. Reson. Ser. A* **1995**, *115*, 273.
[33] R. K. Harris, E. D. Becker, S. M. C. de Menezes, R. Goodfellow, P. Granger, *Pure Appl. Chem.* **2001**, *73*, 1795.
[34] D. Vanderbilt, *Phys. Rev. B* **1990**, *41*, 7892.
[35] J. P. Perdew, K. Burke, M. Ernzerhof, *Phys. Rev. Lett.* **1996**, *77*, 3865.
[36] H. J. Monkhorst, J. D. Pack, *Phys. Rev. B* **1976**, *13*, 5188.
[37] S. Clark, M. Segall, C. Pickard, P. Hasnip, M. Probert, K. Refson, M. Payne, *Z. Kristallogr. Cryst. Mater.* **2005**, *220*, 567.
[38] D. S. Middlemiss, F. Blanc, C. J. Pickard, C. P. Grey, *J. Magn. Reson.* **2010**, *204*, 1.

Manuscript received: December 7, 2023
Revised manuscript received: January 26, 2024
Accepted manuscript online: January 27, 2024
Version of record online: February 23, 2024